

RESEARCH

Open Access



4D quantitative proteomics of ovarian granulosa cells reveals the involvement of oxidative phosphorylation in non-elderly women with diminished ovarian reserve

Hong-xing Li^{1,2,3†}, Xiao-ling Ma^{1,2†}, Li-li Zhang^{1,2}, Tian-yu Jia^{1,2}, Yi Jin^{1,3}, Shi-long Xue^{1,2} and Ya-Ming Xi^{1,3*}

Abstract

Objective This study compared the proteomic differences between non-elderly diminished ovarian reserve (DOR, < 35 years) and normal ovarian reserve (NOR) to better understand the molecular mechanisms behind ovarian reserve changes in Poseidon Group III. **Methods:** Ovarian granulosa cells (GCs) from infertile women with DOR in Poseidon Group III and women with NOR were analyzed using 4D label-free quantitative proteomics. A comprehensive bioinformatics analysis was performed to identify differentially expressed proteins (DEPs) in order to gain a deeper understanding of the mechanisms underlying DOR. The results were subsequently validated by RT-qPCR and Western blot. **Results:** In this study, a total of 4,940 proteins were identified. Compared to the NOR group, the non-elderly DOR group showed 63 upregulated proteins and 308 downregulated proteins. Among the differentially expressed proteins, 77 were localized to the mitochondria, representing 28.62% of the total. Key domains, including Pyridine nucleotide-disulfide oxidoreductase, FAD/NAD(P)-binding, and Acyl-CoA dehydrogenase/oxidase C-terminal, showed the highest enrichment in mitochondria, suggesting mitochondrial dysfunction in diminished ovarian reserve. Gene Ontology (GO) analysis indicated that most differential proteins were involved in oxidoreductase activity, immune processes, and coenzyme binding. Kyoto Encyclopedia of Genes and Genomes (KEGG) pathway analysis highlighted metabolic pathways and oxidative phosphorylation as the most enriched. Furthermore, it was confirmed that the expression of NDUFS3, NDUFB5, NDUFAF2, UQCRC1, UQCRC2, ATP5L, DAG1, PKM2, and SIRT5 matched the proteomics data. **Conclusions:** We present the first data on the protein expression profiles in ovarian GCs from NOR and Poseidon Group III patients using 4D proteomics. The proteins identified in this study could serve as potential novel biomarkers for Poseidon Group III patients.

Keywords Diminished ovarian reserve, Ovarian granulosa cells, Differentially expressed proteins, 4D proteomics, Poseidon Group III

[†]Hong-xing Li and Xiao-ling Ma contributed equally to this work.

*Correspondence:

Ya-Ming Xi

xiyaming01@163.com

Full list of author information is available at the end of the article



Introduction

Infertility, a global issue affecting couples of childbearing ages, is poised to become the third leading health concern following cancer and cardiovascular diseases [1]. Infertility can markedly diminish both quality of life and marital satisfaction. The concept of diminished ovarian reserve (DOR) was initially coined by Navot in 1987 [2]. Defined by elevated follicle-stimulating hormone (FSH) and reduced anti-Müllerian hormone (AMH) levels, DOR manifests clinically through oligomenorrhea, perimenopausal symptoms, and compromised fertility [2, 3]. Currently, the method for assessing ovarian reserve function lacks sufficient accuracy. While DOR is commonly associated with advanced maternal age (≥ 35 years), it increasingly affects younger women (typically < 35 years), with an estimated prevalence of 10–15% in women of reproductive age, though rates vary depending on diagnostic criteria and population studies [4, 5].

DOR often results in poor pregnancy outcomes, primarily manifested as infertility, early abortion, recurrent abortion, poor response to gonadotropin (Gn), and repeated embryo implantation failure. Currently, the etiology of DOR remains unclear [6]. Apart from age, potential contributing factors primarily include genetic, iatrogenic, autoimmune, infectious, and psychosocial elements. Presently, therapeutic strategies remain largely empirical. Early-onset DOR may stem from genetic predispositions (e.g., Fragile X premutation), autoimmune disorders, iatrogenic causes (e.g., chemotherapy), environmental toxins, or idiopathic factors [7, 8]. Assisted reproductive technologies (ART), including tailored controlled ovarian stimulation (COS) protocols and adjuvant therapies (e.g., Coenzyme Q10, dehydroepiandrosterone), show inconsistent efficacy across DOR populations [9–11]. This therapeutic ambiguity underscores critical knowledge gaps in the molecular pathogenesis of DOR, particularly in younger women who represent a growing clinical demographic.

To date, several proteomic studies related to ovarian reserve have been reported. Li et al. utilized isobaric tags for relative and absolute quantification (iTRAQ) technology to identify candidate urinary proteins across three groups: polycystic ovary syndrome (PCOS), DOR, and normal control [12]. Their findings suggested that urinary Vitamin D-binding protein was closely linked to ovarian reserve and may serve as a novel noninvasive biomarker for its assessment. Subsequent investigations of follicular fluid proteomes in Traditional Chinese Medicine KLP-treated DOR patients revealed pathway alterations in fatty acid and purine metabolism [13]. Xu et al. proposed that cigarette smoke extract reduced ovarian reserve in mice by disrupting the CREB1-mediated balance between ovarian granulosa cells (GCs) proliferation and

apoptosis [14]. They identified possible therapeutic targets for clinical intervention in premature ovarian failure (POI) induced by cigarette smoke exposure using liquid chromatography-tandem mass spectrometry quantitative proteomics. Nevertheless, existing proteomic analyses share a critical limitation: none have systematically compared molecular signatures between age-stratified DOR cohorts.

In this study, we conducted 4D label-free proteomic profiling of ovarian GCs from Poseidon Group III DOR patients and normal ovarian reserve (NOR) controls. Through integrated bioinformatics and experimental validation (RT-qPCR and Western blot), we identified differentially expressed proteins (DEPs) that may serve dual roles as diagnostic biomarkers and therapeutic targets for non-age-related DOR. Our findings not only delineate age-specific molecular pathways in DOR but also provide a framework for personalized management of premature ovarian failure.

Methods

Patients and sample collection

Clinical samples were gathered at the Reproductive Center, the First Hospital of Lanzhou University, spanning from September 2020 to February 2024. A total of 160 patients were recruited in this study. These patients underwent Intracytoplasmic sperm injection (ICSI) with gonadotrophin-releasing hormone (GnRH) antagonist for controlled ovarian hyperstimulation. Based on Bologna and Poseidon classification, the modified inclusion criteria (Poseidon Group III) were as follows: aged 25–35 years; antral follicle count < 5 ; anti-Müllerian hormone < 1.2 $\mu\text{g/L}$; body mass index (BMI) ranging from 18–25 kg/m^2 ; and no prior occurrences of endocrine disease, uterine anomaly, or chromosomal abnormalities [15]. This study was approved by the Ethics Research Committee, the First Hospital of Lanzhou University, China (No. LDYYLL2019-42).

The study group consisted of eighty non-elderly infertile women diagnosed with DOR. The control group, consisting of eighty NOR infertility women with the same GnRH antagonist ovarian hyperstimulation during the same period of time, attributed solely to male factors such as azoospermia or severe oligospermia/ aspermia. Because single-patient granulocyte samples were too few to complete the proteomic test, we concentrated samples from 12–15 individuals as a group. Randomization was performed using serial numbers generated by the widely adopted online randomization tool (website <https://www.randomizer.org/>, version 4.0) to assign corresponding groups [16]. For proteomic analysis, the total number of oocyte-cumulus-corona complexes (OCCCs) in each pooled group was

balanced. At last, forty patient samples were selected randomly for proteomic analysis, while the remaining forty underwent RT-qPCR, ATP assay and western blot.

Controlled ovarian stimulation protocol was summarized as follows: starting from the 2nd day of the menstrual cycle, intramuscular injection of human menopausal gonadotropin (HMG, Livzon, China) or gonadotropin (Merck Serono, Switzerland) at a dosage of 200 to 300 IU/day, adjusted according to patient demographics such as age, body mass index (BMI), antral follicle count (AFC), and previous ovulation induction experiences. When the average follicle diameter reached 12 to 14 mm, the antagonist Cetrorik Acetate was injected subcutaneously (Stercax, Merck Serono). When two or more dominant follicles exceeded 16 to 18 mm in diameter, a trigger was administered involved human chorionic gonadotropin (hCG, Livzon). Ultrasound-guided follicular aspiration was performed 36 h after ovulation induction [17].

GCs were purified from follicular fluid by density gradient centrifugation [18]. After initial centrifugation at $380 \times g$ for 5 min, the precipitate was resuspended in PBS. Then, the suspension was gently layered onto the Ficoll-Paque, followed by centrifugation at $380 \times g$ for 20 min. The GC layer was aspirated into a 1.5 mL tube and centrifuged for another 5 min. Besides, cumulus granulosa cells were harvested from oocyte-cumulus complexes after digestion with hyaluronidase and washed three times with PBS. Finally, the GCs were stored at -80°C for further analysis.

Protein extraction

Samples were transferred to 1.5 mL centrifuge tubes. An appropriate amount of protein dissolution solution (8 M urea [Sinopharm, Cat. No. 10023218], 100 mM triethylammonium bicarbonate [TEAB, Sigma-Aldrich, Cat. No. T7408-500ML], pH = 8.5) was added. The samples were subjected to ultrasonication in an ice-water bath for 5 min for complete lysis. After centrifugation at 12000 g for 15 min, the supernatant was collected and an appropriate amount of 1 M dithiothreitol (DTT, Sigma-Aldrich, Cat. No. D9163) was added for a 1-h reaction at 56°C , followed by a 2-min ice bath. Subsequently, a sufficient amount of iodoacetamide (IAM, Sigma-Aldrich, Cat. No. I6125) was added, and the reaction was carried out in the dark for 1 h. The amount of protein was measured using the Bradford protein quantification reagent kit (Servicebio, Cat. No. G2001-250ML). Construct a standard curve using the absorbance at 595 nm of the standard protein solution and calculate the protein concentration of the test samples following the kit instructions.

Protein digestion

The protein suspension was added trypsin (Promega, Cat. No. V5280) and 100 mM TEAB buffer and incubated at 37°C for 4 h for enzymatic digestion. Then, trypsin and Calcium chloride (CaCl_2 , Sigma-Aldrich, Cat. No. 10043-52-4) were added for overnight digestion. The digestion supernatant peptides were separated by vacuum centrifugation (12000 g) and desalted using C18 column (Sigma-Aldrich, Cat. No. 50204-U). The washing solution and eluent solution were as follows: 0.1% formic acid (Thermo Fisher Scientific, Cat. No. A117-50)/3% acetonitrile (Thermo Fisher Scientific, Cat. No. A955-4), 0.1% formic acid/70% acetonitrile, respectively. The number of peptides was measured by measuring the UV spectral density at 280 nm.

Liquid chromatography-mass spectrometry (LC-MS)

Dissolve the lyophilized peptides powder and centrifuge at 14,000 g for 20 min. Then the supernatant samples were detected by LC-MS analysis using the tims TOF Pro2 mass spectrometer with a Captive Spray ion source (Bruker, USA). The ion spray voltage was set 1.5 kV. Perform a full scan in the mass range of m/z 100–1700 with a ramp time of 100 ms and a Lock Duty Cycle of 100%. Utilize Parallel Accumulation Serial Fragmentation (PASEF) settings with 10 MS/MS scans (total cycle time of 1.17 s). The threshold of Ion intensity was 2500, and the scheduling target intensity was 20,000. Collect the raw mass spectrometry data in the .d file format for further analysis.

Proteomic data analysis

Perform a comprehensive analysis of all result spectra using the MaxQuant search software (Bruker, version MQ2.2). The MaxQuant search parameters were set as follows: a mass tolerance of 20 ppm for precursor ions and 0.05 Da for-fragment ions. Fixed modifications included alkylation on cysteine residues, while variable modifications encompassed methionine oxidation. According to software Settings, up to 2 missed cleavage sites were allowed.

In order to improve the reliability of the analysis results, Peptide Spectrum Matches (PSMs) with a credibility of over 99% were considered trustworthy. And proteins with at least one unique peptide segment were required for further analysis. Only reliable peptide spectra and proteins were retained. Peptide segments and proteins with an FDR greater than 1% were eliminated. A T-test was employed for statistical analysis of protein quantification results. Experimental and control group proteins with significant quantitative differences ($p < 0.05$, $|\log_2\text{FC}| > 1.5$) were defined as differentially expressed proteins

(DEPs). The annotation of Gene Ontology (GO) was carried out using the InterProScan software (EMBL-EBI, version 5.22–61.0) and Metascape database (<http://metascape.org/>, version v3.5). Functional protein pathway analyses were conducted for the identified proteins using Kyoto Encyclopedia of Genes and Genomes (KEGG) databases. Thresholds for GO and KEGG enrichment analysis visualization were set as follows: False discovery rate (FDR) < 0.05, Gene set size ≥ 5 and Enrichment factor (EF) > 1.5. Gene sets with > 500 genes were excluded to minimize nonspecific associations. Gene set enrichment analysis (GSEA) was performed using the Hallmark gene sets (MSigDB, version 2023.1) with thresholds of $|\text{NES}| > 1.5$, FDR < 0.25. Gene sets with 15–500 genes were retained.

Constructing the protein–protein interaction (PPI) network of DEPs

The above DEPs were imported into String database (<https://cn.string-db.org/>, version 12.0) and Metascape database to generate PPI network, as previously described [19]. The PPI network map was generated from Cytoscape (software version 3.9.1). Calculating the Degree value of each node in the protein network graph through Cytoscape Network Analysis. Furthermore, the MCODE algorithm in Cytoscape was used to find several closely connected protein clusters from the complex targets network and the biological functions of each protein cluster were labeled. MCODE parameters: Degree Cutoff = 2, Node Score Cutoff = 0.2, Max Depth = 100, Haircut enabled, Fluff disabled, and K-Core = 2.

RNA extraction and qPCR analysis

Trizol Reagent (Invitrogen, Cat. No. 15596026 CN) was used to extract total RNA. Complementary DNA was synthesized by PrimeScript RT reagent Kit (Takara, Cat. No. RR047 A). Real-time quantitative PCR was performed with BeyoFast SYBR Green qPCR Mix (Beyotime, Cat. No. D7260). Three independent biological replicates were employed for validation experiments. The sequence of all primers in this study was shown in Supplementary Table 1.

Western blot analysis

Total protein samples were obtained from frozen ovarian GCs, and protein concentration was evaluated by the BCA technique (Beyotime, Cat. No. P0010). In short, protein extracts were separated by electrophoresis of 10% sodium dodecyl sulfate polyacrylamide gel and transferred to polyvinylidene fluoride (PVDF) membranes (Sigma-Aldrich, Cat. No. IPVH00010). Anti-NDUFAF2 (20kda), anti-ATP5L (55kda), anti-PKM2 (58kda) and anti-DAG1 (98kda) were purchased from BiossChina

(Cat. No. bs-6551R, bs-107290P, bsm-61301R, bs-4075R, respectively) and incubated overnight at 4°C. Specific horseradish peroxidase linked IgG (Tiangen, Cat. No. PA112-02) was used to incubate at room temperature for 2 h. ImageJ (version 2.9.0) was employed for data analysis. GAPDH and β -actin were used as an internal control.

Adenosine triphosphate (ATP) assay

Enhanced ATP Assay Kit (Beyotime, Cat. No. S0027) was used to measure ATP levels in GCs cells. Briefly, The ATP standard curve was assessed based on different proportions of ATP standard solution and ATP detection cracking solution. Then the ATP concentration of the sample was calculated according to the standard curve. Since differences in protein concentration during sample preparation can lead to inaccuracies in ATP levels, this experiment first measures the protein concentration in the GC cells and then expresses the ATP content as nmol of ATP per mg of protein.

Results

Differential proteins analysis

In this experiment, we conducted proteomic research on granulosa cells from pre-ovulatory follicles of non-elderly patients undergoing controlled ovarian stimulation with DOR and NOR, based on 4D-label-free technology. Finally, a total of 157,445 matched spectra, 40,105 peptides, and 4,940 identified proteins were obtained. PCA analysis of proteomics results was shown in the Supplementary Figure S1. The comprehensive overview of protein identification in the samples can be found in Supplementary Table 2. The relative quantification values of each PSM in each sample based on the peak area of the original spectra were collected by the software Proteome Discoverer. Subsequently, the relative quantification values of proteins were obtained based on the quantification information of all PSMs contained in the identified unique peptide segments. The protein quantification results are shown in Supplementary Table 3.

In this study, differential proteins between the DOR group and the NOR group were screened. Among them, there were 63 upregulated proteins and 308 downregulated proteins (Supplementary Table 4). The top 10 upregulated and downregulated proteins were listed in Table 1. The volcano map and clustering heat map of differential proteins were shown in Fig. 1. The dendrogram illustrated distinct clustering patterns between groups, highlighting systemic proteomic dysregulation in DOR.

Enrichment analysis

The Gene Ontology (GO) database can provide standardized vocabulary for describing gene and protein functions. The total number of 207 GO terms was annotated

Table 1 The top 10 upregulated and downregulated proteins of the proteomics (DOR.vs.NOR)

Protein ID	Description	Gene	FC	Pvalue	log2 FC	Up/Down
Q96SB3	Neurabin-2	PPP1R9B	0.09	0.043	-3.43	down
O75438	NADH dehydrogenase 1 beta subcomplex subunit 1	NDUFB1	0.09	0.001	-3.37	down
Q9NWU1	3-oxoacyl-[acyl-carrier-protein] synthase	OXSM	0.15	0.014	-2.75	down
Q8IVS2	Malonyl-CoA-acyl carrier protein transacylase	MCAT	0.18	0.007	-2.50	down
Q9BQE5	Apolipoprotein L2	APOL2	0.19	0.003	-2.43	down
P18054	Polyunsaturated fatty acid lipoxigenase ALOX12	ALOX12	0.19	0.021	-2.40	down
A0A6Q8PHM8	Alpha-galactosidase	GLA	0.20	0.001	-2.30	down
B7ZKY8	ADP-ribosylation factor related protein 1	ARFRP1	0.21	0.008	-2.26	down
D6RA56	NADH dehydrogenase 1 alpha subcomplex assembly factor 2	NDUFAF2	0.23	0.031	-2.10	down
Q53HG1	NADH dehydrogenase 1 alpha subcomplex subunit 12	NDUFA12	0.25	0.028	-2.01	down
H0YNX7	GTP cyclohydrolase 1 feedback regulatory protein	GCHFR	10.29	0.008	4.34	up
Q6J1Z9	Hemoglobin alpha 1	HBA1	5.06	0.029	2.34	up
Q6RFH5	WD repeat-containing protein 74	WDR74	4.72	0.023	2.24	up
Q9P2E9	ribosome binding protein 1	RRBP1	3.86	0.044	1.95	up
H0Y5B4	60S ribosomal protein L36a	RPL36A	3.54	0.009	1.93	up
A0A0S2Z4C5	Protein S100	S100B	3.49	0.029	1.90	up
A0A385HW02	hemoglobin alpha 2	HBA2	3.17	0.018	1.76	up
A8K6Q3	Synaptic vesicle glycoprotein 2A	SV2A	3.07	0.020	1.72	up
P43652	Afamin	AFM	2.77	0.001	1.67	up
A8K9S3	Coronin 1 A	CORO1A	2.75	0.016	1.66	up

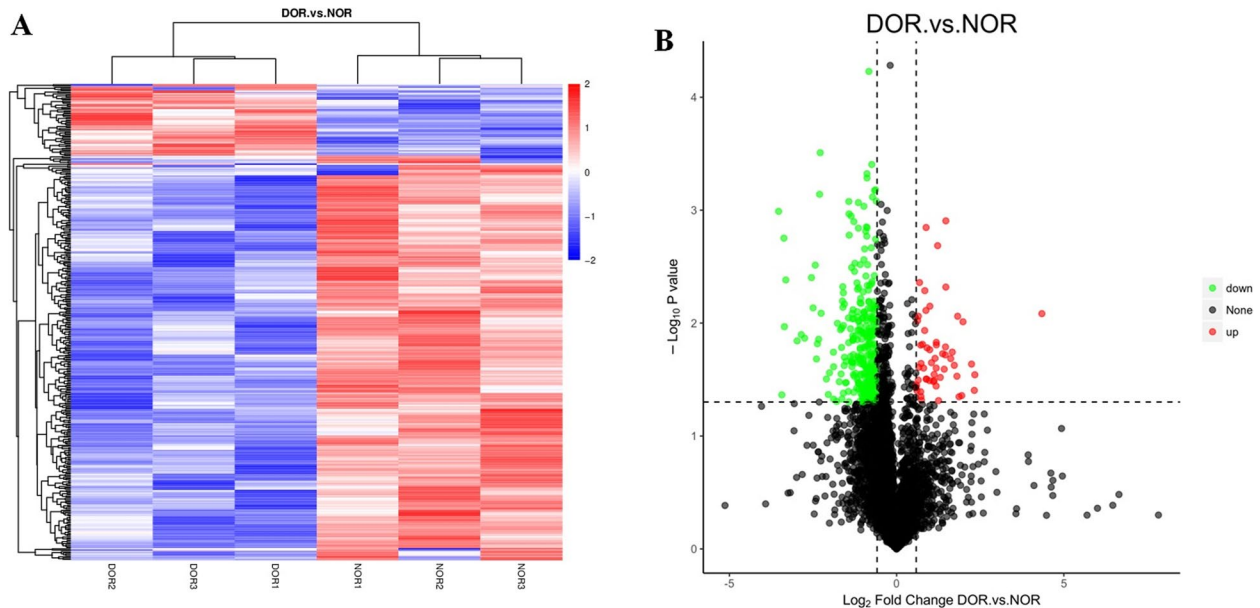


Fig. 1 Proteomic profiling of differential proteins between the DOR and NOR groups. **A** hierarchical clustering heatmap of DEPs across DOR and NOR samples. Rows represent proteins, and columns represent individual samples. Color intensity reflects Z-score-normalized protein abundance (red: upregulated; blue: downregulated). The dendrogram illustrates distinct clustering patterns between groups. **B** Volcano plot visualizing the statistical significance versus magnitude of change for all quantified proteins. Red dots denote significantly upregulated protein, blue dots represent downregulated proteins

in this study, including 99 biological process (BP) terms, 54 cellular component terms (CC) and 54 molecular function (MF) terms (Refer to Supplementary Table 5). The GO functional analysis revealed that most of the differential proteins were involved in oxidoreductase activity, metabolic process and oxidation–reduction process (Fig. 2A–D). Top 3 significantly enriched terms of the biological process included proton transmembrane transport (GO:1,902,600, FDR = 2.13×10^{-6}), proton motive force-driven mitochondrial ATP synthesis (GO:0042776, FDR = 1.77×10^{-10}) and aerobic respiration (GO:0009060, FDR = 6.23×10^{-8}).

KEGG pathway analysis of the differential proteins suggested that the most enriched pathways were those involved in metabolic pathways (hsa01100, FDR = 1.06×10^{-14}) and oxidative phosphorylation (hsa00190, FDR = 1.86×10^{-10}) (Fig. 2E). In addition, Gene Set Enrichment Analysis (GSEA) analysis was performed in this study. The most significant difference in GSEA analysis was also for oxidation–reduction process (Fig. 2C and Supplementary Table 6).

Proteomic domain and subcellular localization analysis

Structural domain enrichment analysis can be used to understand the function of differential proteins and identify certain genes associated with diseases. InterProScan is one of the commonly used software for protein structural domain and functional annotation. The IPR enrichment results of differential proteins were shown in Supplementary Table 7. Based on the enrichment results mentioned above, a bubble chart of enriched structural domains was generated (Fig. 3A). Meanwhile, the subcellular localization proportion of differential proteins was analyzed, as shown in (Fig. 3B). Among all differential proteins, a total of 77 proteins were concentrated in the mitochondria, accounting for 28.62% of the total. GSEA analysis similarly confirmed this result (Fig. 3C). According to the above results, the Pyridine nucleotide-disulphide oxidoreductase, FAD/NAD(P)-binding domain, and Acyl-CoA dehydrogenase/oxidase C-terminal exhibited the highest enrichment levels among differential proteins. These domains were predominantly found in mitochondria, indicating the involvement of mitochondrial dysfunction in diminished ovarian reserve.

PPI network analysis based on MCODE module

The differential proteins were imported into the String database, and the confidence level was set to 0.7. Isolated targets were removed, and the network was visualized and analyzed by Cytoscape to construct the protein interaction network based on MCODE module. The proteins in the modules were subsequently scored and clustered according to the degree of association. The interaction of module clusters was mapped by ClusterViz in Cytoscape, as described in Fig. 4A. The network layout from Metascape database was shown in Supplementary Figure S2. The GO analyses of the largest protein clusters suggested that these targets were related to the mitochondrial matrix and oxidoreductase activity (Fig. 4B).

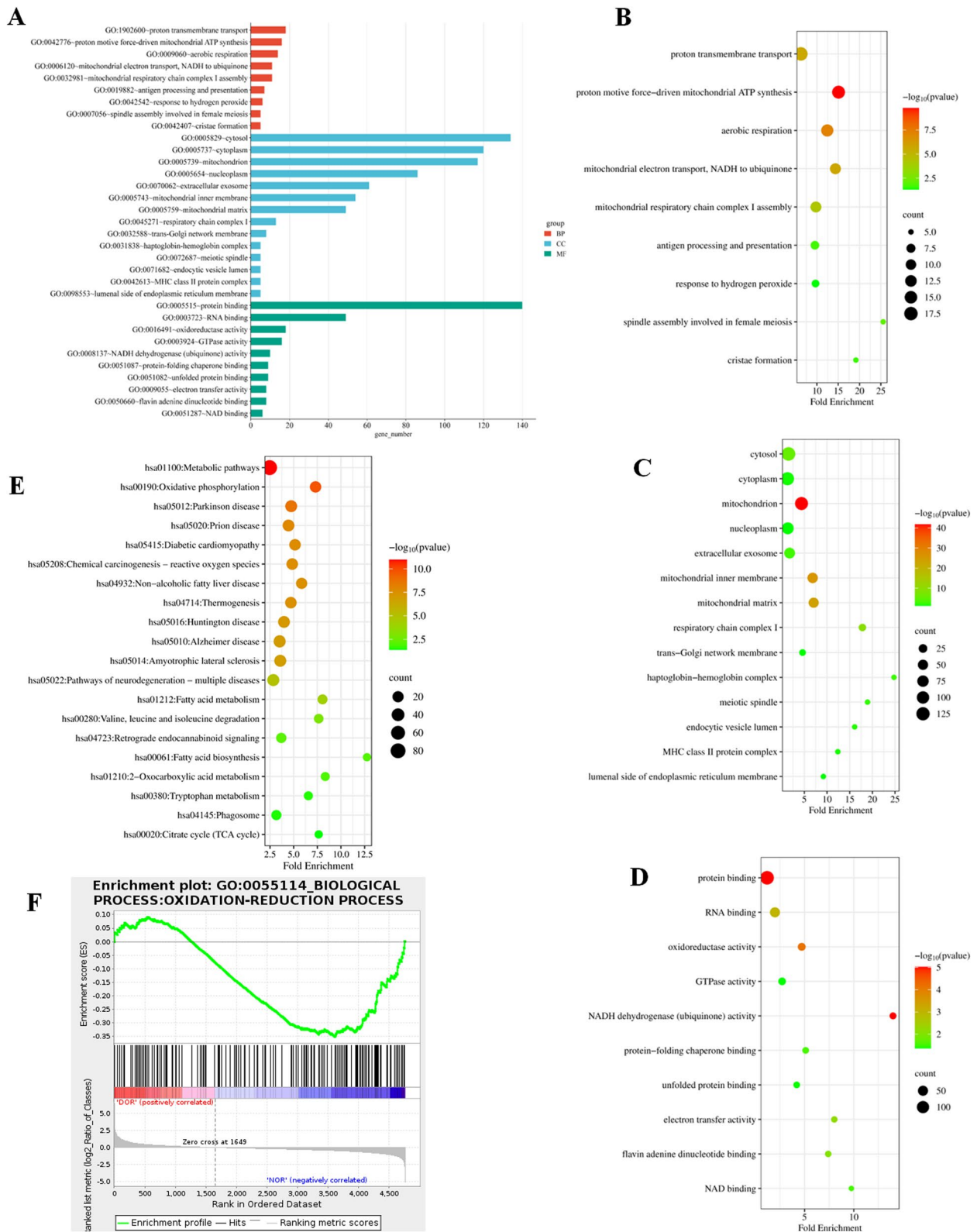
Experimental validation of bioinformatics results

Based on the above bioinformatics analysis, the expression of several key genes for oxidative phosphorylation was measured. The mRNA expression levels of NDUFS3 (NADH:ubiquinone oxidoreductase core subunit S3), NDUFB5 (NADH:ubiquinone oxidoreductase subunit B5), NDUFAF2 (NADH:ubiquinone oxidoreductase complex assembly factor 2), UQCRC1 (ubiquinol-cytochrome c reductase core protein 1), UQCRC2 (ubiquinol-cytochrome c reductase core protein 2), ATP5L (ATP synthase membrane subunit g), DAG1 (dystroglycan 1), SIRT5 (sirtuin 5) and HIBADH (3-hydroxyisobutyrate dehydrogenase) decreased notably in non-elderly DOR compared with NOR (Fig. 5A). However, the expression of PKM2, a key enzyme in glycolysis, did not change between the two groups. Interestingly, DAG1 expression was significantly reduced in the DOR group. Western blot results were consistent with those obtained from qRT-PCR (Fig. 5B). Collectively, these results confirmed that oxidative phosphorylation was involved in diminished ovarian reserve in non-elderly patients.

ATP synthesis is one of the main functions of mitochondria. The intracellular ATP concentration showed that the average ATP level in granular cells of non-elderly DOR group was significantly lower than that of NOR group. Previous studies have shown that coenzyme Q10 may be a promising supplement for improving DOR [20, 21]. In this study, treatment of non-elderly DOR granulosa cells with Coenzyme Q10 and L-carnitine together significantly promoted ATP synthesis (Fig. 5C).

(See figure on next page.)

Fig. 2 Functional Enrichment Analysis of DEPs between the DOR and NOR Groups. **A** Histogram of GO enrichment analysis for DEPs in the BP, CC and MF category. **B, C, D, E** Scatter plot of the BP, CC, MF and KEGG pathway enrichment analysis, respectively. The horizontal axis represented the Fold Enrichment, while the vertical axis represented the enriched pathway name. Only gene sets with ≥ 5 proteins were shown. **F** GSEA of DEPs showed that oxidation–reduction process exhibited the most statistically remarkable enrichment (normalized enrichment score [NES] = -1.55 , adjusted p -value < 0.001)



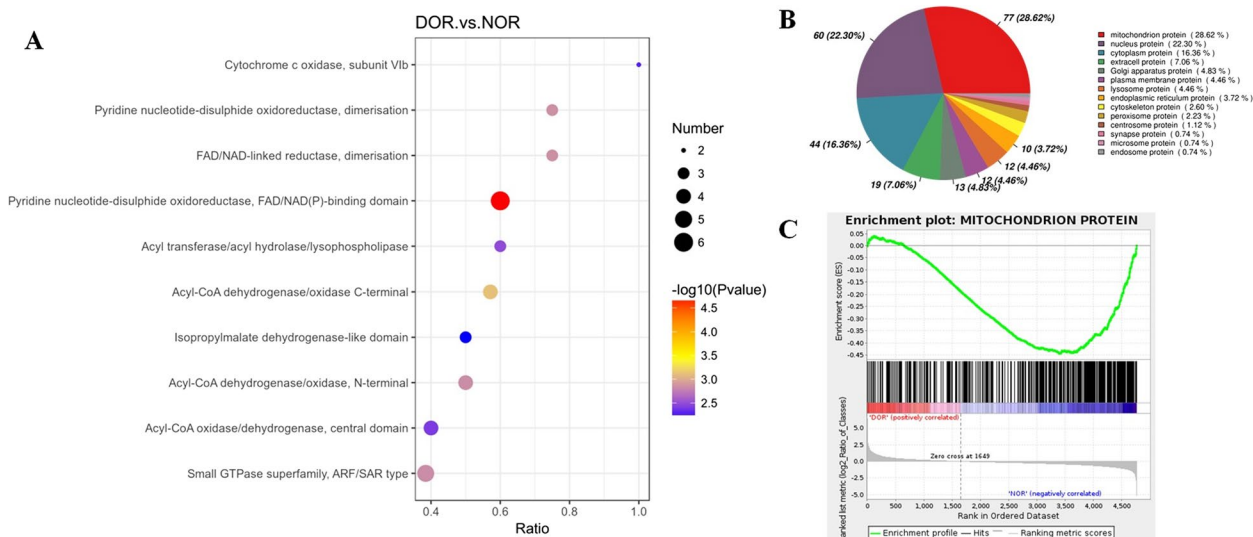


Fig. 3 Domain annotation and subcellular localization of DEPs. **A** Protein structural domain enrichment analysis of DEPs using the InterPro database. Among all enrichment results, the pyridine nucleotide-disulphide oxidoreductase, FAD/NAD(P)-binding domain (IPRO23753, adjusted p -value = 2.10×10^{-5}) exhibited the most significant enrichment. **B** Subcellular localization prediction of DEP. The majority of DEPs localized to the mitochondria (28.62%), followed by nucleus (22.30%) and cytoplasm (16.36%), implicating mitochondrial dysfunction in the disease phenotype. **C** GSEA of subcellular localized DEPs demonstrated that mitochondrial proteins exhibited the most statistically significant enrichment (NES = -1.85, adjusted p -value < 0.001)

Collectively, the results substantiated the involvement of oxidative phosphorylation in non-elderly women with DOR.

Discussion

Implemented through the tims-TOF Pro mass spectrometry platform, 4D proteomics employs dual trapped ion mobility spectrometry (TIMS) combined with the innovative Parallel Accumulation-Serial Fragmentation (PASEF) technology. This advanced configuration significantly enhances protein identification throughput and quantification accuracy while reducing sample requirements to the sub-microgram level [22]. Leveraging 4D proteomics, we identified 371 differential proteins between the DOR and the NOR group, with a predominant enrichment in metabolic pathways and oxidative phosphorylation.

In clinical practice, it was often found that chronological age was not equal to biological ovarian age. In non-elderly patients with DOR, the number of follicles in the ovaries was reduced, and the quality of oocytes declined [18, 23]. Oocyte development relied on granulosa cells, which were divided into cumulus granulosa cells and mural granulosa cell. Cumulus GCs were the only somatic cells that directly contacted the oocyte, providing essential growth factors, hormones, and other nutrients. Therefore, granulosa cells were regarded as the best non-invasive method for assessing oocyte or embryo quality.

This study suggests that abnormal oxidative phosphorylation was involved in decreased ovarian reserve in non-elderly patients. According to the subcellular localization analysis of all the differential proteins, a total of 77 proteins were concentrated in mitochondria, accounting for 28.62% of the total. Mitochondria not only supplied the energy necessary for the proliferation and metabolism of GCs but also played a critical role in regulating essential physiological processes such as antioxidative defense, apoptosis, and autophagy. It was reported that mitochondrial dysfunction can lead to the generation of reactive oxygen species (ROS), the release of pro-apoptotic factors (such as cytochrome c), and the activation of apoptotic proteases and endonucleases [24]. Based on our protein structural domain annotation, the pyridine nucleotide-disulphide oxidoreductase, FAD/NAD(P)-binding domain exhibited the most significant enrichment. Knockout of Pyridine Nucleotide-Disulphide Oxidoreductase Domain can decreased Mitochondrial Membrane Potential, complex IV activity, cell proliferation and ATP content, but increased mtROS levels and the number of immature mitochondria [25], suggesting the correlation between non-elderly DOR and mitochondrial dysfunction.

The ATP required by granulosa cells was predominantly generated through oxidative phosphorylation (OXPHOS) occurring within the mitochondria. The electron transport chain (ETC) relied on critical genes encoding structural and regulatory subunits of its

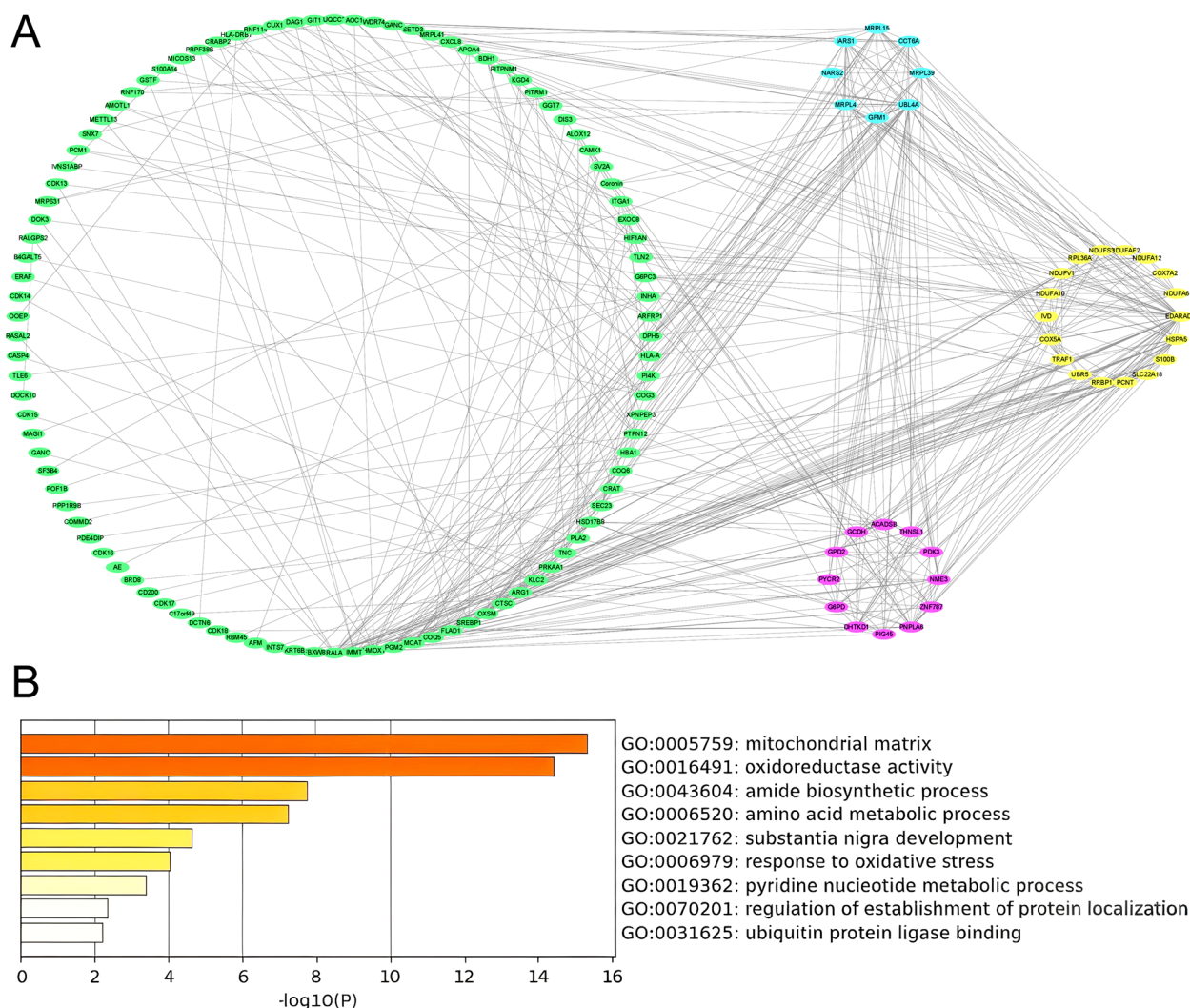


Fig. 4 PPI network analysis of DEPs. **A** The network was constructed using the STRING database (confidence score ≥ 0.7) and visualized in Cytoscape. **B** GO enrichment analysis of the top two protein clusters based on MCODE algorithm. Significantly enriched biological processes included “mitochondrial matrix” (GO:0005759), followed by “oxidoreductase activity” (GO:0016491), and “amide biosynthetic process” (GO:0043604)

complexes. NDUF53 and NDUF55 were essential subunits of Complex I (NADH:ubiquinone oxidoreductase), where NDUF53 facilitated electron transfer from NADH to ubiquinone and stabilizes the complex, while NDUF55 supported proton translocation and structural integrity [26, 27]. NDUF62, a chaperone for Complex I assembly, ensured proper subunit incorporation, with mutations causing early-onset cardiomyopathy [28]. In Complex III (ubiquinol-cytochrome c reductase), UQCRC1 and UQCRC2 formed the core structure, mediating electron transfer from ubiquinol to cytochrome c and maintaining complex stability, with variants associated with metabolic dysfunction [29]. Finally, ATP5L, a stator stalk subunit of Complex V (ATP synthase), couples proton flow to ATP synthesis, and its dysfunction contributes

to mitochondrial encephalopathies [30]. Besides, SIRT5, a mitochondrial NAD-dependent deacylase, regulated lysine succinylation, malonylation, and glutarylation, modulating metabolic pathways such as fatty acid oxidation, amino acid metabolism, and the mitochondrial unfolded protein response [31]. HIBADH, a key enzyme in valine catabolism, converted 3-hydroxyisobutyrate to methylmalonate semialdehyde [32]. Both genes were critical for maintaining mitochondrial metabolic homeostasis, with emerging therapeutic implications. All these genes collectively underpinned mitochondrial bioenergetics, and their impairment highlighted molecular mechanisms driving metabolic disorders [33].

During oocyte and embryo development, insufficient ATP levels can lead to an increase in aneuploidy,

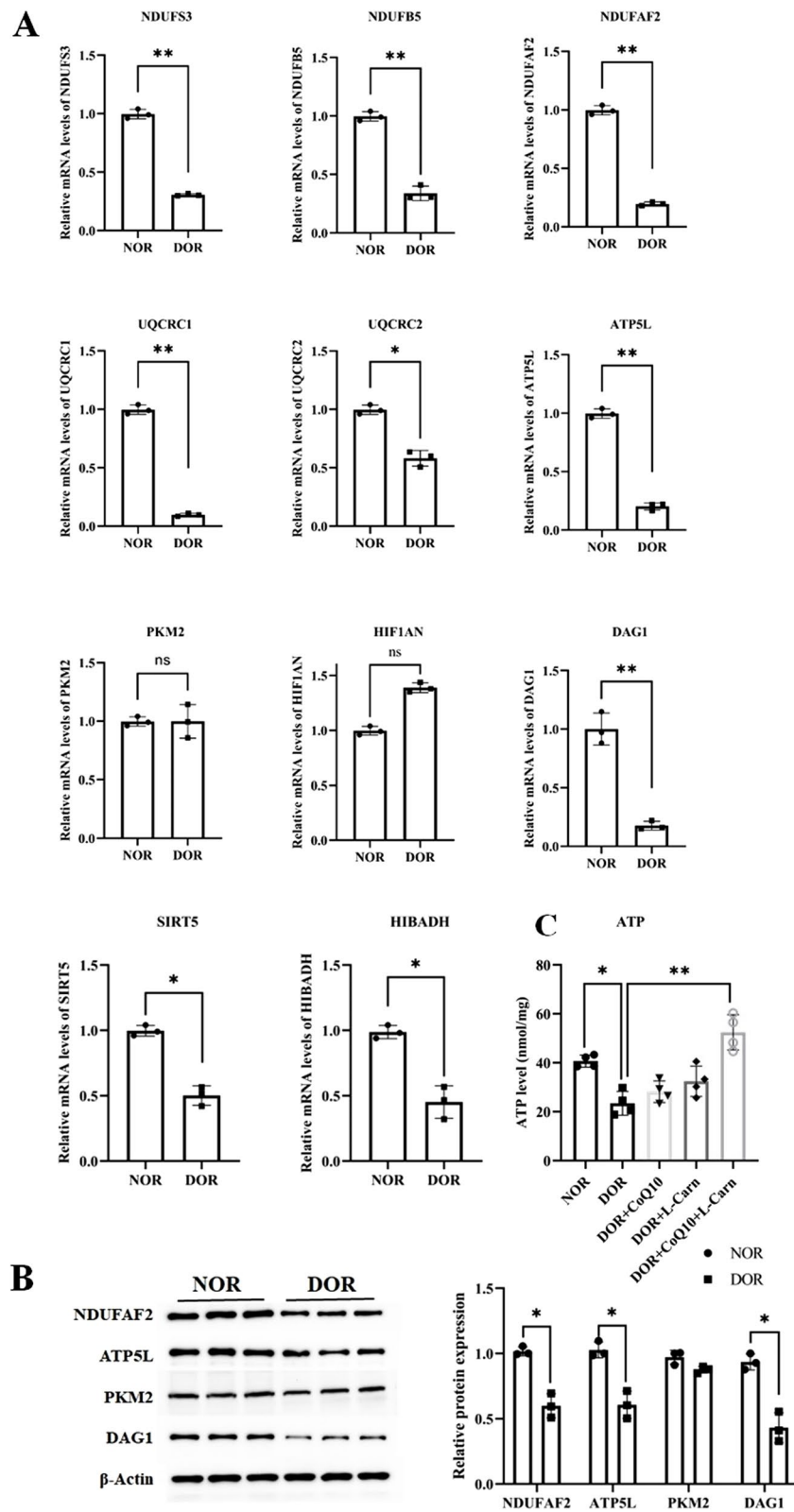


Fig. 5 qRT-PCR and Western blot validation of proteomics results. **A** The mRNA expressions of NDUF3, NDUF5, NDUF2, UQCRC1, UQCRC2, UQCRC2, ATP5L, PKM2, DAG1, SIRT5 and HIBADH of non-elderly DOR and control groups by qRT-PCR. **B** The protein expression of NDUF2, ATP5L, PKM2 and DAG1 by Western blot. **C** Intracellular ATP concentration measurement

resulting in abnormal chromosome segregation [34]. Our research has demonstrated that, compared to the NOR group, younger DOR individuals exhibited significantly lower expression levels of all of these above gene. The findings of this study suggested that the reduced fertility observed in non-elderly patients with DOR was, to some extent, associated with dysfunction in the mitochondrial function of granulosa cells. To clarify the molecular mechanisms of protein expression in GCs from non-elderly DOR and NOR, PPI data were retrieved from the STRING online database. STRING was an open-source tool for predicting and visualizing complex networks. Our findings demonstrated that these proteins were implicated in mitochondrial matrix and oxidoreductase activity involved in follicle development. Interestingly, the expression of the glycolysis-related gene PKM2 was not affected. Thus, enhancing OXPHOS function in granulosa cells may represent a critical avenue for addressing infertility in non-elder women.

Qin et al. reported alternative splicing (AS) events during oocyte maturation in vivo and in vitro, with OXPHOS pathway genes (NDUFA7, NDUFS5, NDUFB1) showing AS alterations [35]. Notably, our study found significant downregulation of NDUFB1 in the non-elderly DOR group, accompanied by reduced expression of splicing regulators Pre-mRNA-splicing factor 38B (PRPF38B) and splicing factor 3b subunit 4 (SF3B4) (Supplementary Table 4). These concurrent changes imply compromised AS regulation in non-elderly DOR cohorts.

DAG1 gene encoded dystroglycan, a central component of dystrophin-glycoprotein complex that linked the extracellular matrix and the cytoskeleton in reproductive tissues. Abnormal DAG1 expression can affect cell migration by influencing filopodia length [36]. In female reproduction, DAG1 was essential for folliculogenesis, oocyte-somatic cell communication, and uterine stromal cell decidualization during embryo implantation [37]. For the first time, we found that the expression of the DAG1 gene was significantly lower in non-elderly DOR than in the control group. Consistent with this, primary cell culture revealed obviously fewer filopodia in the DOR group than in the control group (Supplementary Figure S3), suggesting that this gene may be involved in the progression of non-elderly DOR.

WDR74, a pre-60S ribosome maturation factor, was found to be important for ribosome biogenesis and cell division. WDR74 overexpression disrupted ribosome biogenesis by inducing stoichiometric imbalance of ribosomal large subunit (RPL) proteins and impaired progression beyond the morula stage [38]. Interestingly, besides WDR74, ribosome-binding protein 1 (RRBP1) and 60S ribosomal protein L36a (RPL36 A) also showed elevated expression in our non-elderly DOR group, suggesting a

potential association with poor embryonic developmental potential in some DOR patients.

The variability in DOR group primarily stems from diverse pathophysiological mechanisms (mitochondrial dysfunction, dysregulated hormone signaling, apoptosis/autophagy imbalance) and external confounding factors (gonadotropin stimulation, sample processing inconsistencies) [39, 40]. Notably, ovarian granulosa cells also exhibit obvious heterogeneity, such as mixed granulosa cells from different developmental stages and functional subgroups [41]. The impact of this heterogeneity on differential protein analysis manifests in two aspects: high intra-group variability may mask true differences and non-stratified analyses may overlook subgroup-specific proteins. To address these challenges, this study focused on non-elderly DOR population under uniform controlled ovarian stimulation protocol. Future studies should expand sample sizes and rigorously integrate cohort stratification, multi-omics data, and machine learning algorithms to identify differential proteins independent of confounding factors.

Granulosa cells were essential during key stages of oocyte growth and development, including follicular growth, ovulation, fertilization, and post-FSH stimulation. For all we know, no reports were found that specifically address the protein expression profiles of granulosa cells from non-elderly DOR (< 35 years). One reason for this may be the limited number of cells provided by DOR, which was insufficient for comprehensive proteomics analysis. Here, due to insufficient granulosa cells from individual patients for direct analysis, pooled sample testing was employed. While this approach was necessary for technical feasibility, we acknowledge that it may reduce sensitivity to individual variations. Theoretically, the GCs proteome of a single patient was more reflective of the characteristics of non-elderly DOR, which was a major shortcoming of this study. Future studies with larger unpooled cohorts will further validate these findings.

Current studies often focused on advanced maternal populations, leaving non-elderly-related DOR understudied. Longitudinal cohort studies and multidisciplinary approaches (e.g., genomics, metabolomics) were needed to refine diagnostic criteria, predict progression, and personalize therapies. Addressing these gaps will empower clinicians to better support young women with DOR, ultimately improving reproductive autonomy and quality of life. Our data indicated that certain differentially DEPs may be linked to the details of DOR and oocyte developmental competence. However, the functional roles of some DEPs remain undefined. These proteomics results constituted preliminary data and necessitated further investigation to fully elucidate the roles of the DEPs in follicle development associated with DOR.

Supplementary Information

The online version contains supplementary material available at <https://doi.org/10.1186/s13048-025-01688-1>.

Supplementary Material 1: Supplementary Figure S1. PCA analysis of the DOR and NOR groups. Supplementary Figure S2. The DEPs network layout using Metascape database. Supplementary Figure S3. The morphology of primary cultured granulosa cells. The DOR group exhibited obviously fewer filopodia compared to the control NOR group. Supplementary Table 1. The sequence of all primers in this study. Supplementary Table 2. The comprehensive overview of protein identification in the study. Supplementary Table 3. The protein quantification results of the DOR and NOR groups. Supplementary Table 4. The DEPs identified by proteomics. There were 63 upregulated proteins and 308 downregulated proteins. Supplementary Table 5. GO enrichment analysis of DEPs. Supplementary Table 6. GSEA identified redox-related pathways as the most significantly enriched gene sets. Supplementary Table 7. The IPR enrichment results of differential proteins.

Supplementary Material 2.

Authors' contributions

Hong-xing Li: Investigation, Methodology, Data acquisition and Writing. Xiao-ling Ma: Statistic analysis, Validation and Manuscript drafting. Li-li Zhang: Image processing, Collecting materials. Tian-yu Jia: Manuscript guidance, Revision. Yi Jin: Acquisition, Analysis. Shi-long Xue and Li-li Zhang: Resources, Validation. Ya-ming Xi: Administrative, Material support, Supervision. All authors reviewed the manuscript.

Funding

This work was supported by the Scientific Research Fund of the First Hospital of Lanzhou University (No. ldyyn2021-15), the Natural Science Project of Gansu Province (No. 24JRRA1082, 21JR7RA391) and the Key Research and Development Project of Gansu Province (No. 22YF7FA084). There are no financial or nonfinancial interests that are directly or indirectly related to the work submitted for publication.

Data availability

Data is provided within the manuscript or supplementary information files.

Declarations

Competing interests

The authors declare no competing interests.

Author details

¹The First School of Clinical Medicine, Lanzhou University, Lanzhou 730000, China. ²Clinical Medical Research Center for Reproductive Diseases of Gansu Province, Lanzhou 730000, China. ³Division of Hematology, The First Hospital of Lanzhou University, Lanzhou 730000, China.

Received: 29 March 2025 Accepted: 7 May 2025

Published online: 20 May 2025

References

- Phillips K, Olanrewaju RA, Omole F. Infertility: evaluation and management. *Am Fam Physician*. 2023;107(6):623–30.
- Navot D, Rosenwaks Z, Margalioth EJ. Prognostic assessment of female fecundity. *Lancet*. 1987;2(8560):645–7.
- Zhu Q, Li Y, Ma J, Ma H, Liang X. Potential factors result in diminished ovarian reserve: a comprehensive review. *J Ovarian Res*. 2023;16(1):208.
- Harris BS, Jukic AM, Truong T, Nagle CT, Erkanli A, Steiner AZ. Markers of ovarian reserve as predictors of future fertility. *Fertil Steril*. 2023;119(1):99–106.
- Practice Committee of the American Society for Reproductive Medicine. Testing and interpreting measures of ovarian reserve: a committee opinion. *Fertil Steril*. 2020;114(6):1151–1157.
- Jiang Z, Jin L, Shi W, Xi J, Hu Y, Liu X, et al. A combination of follicle stimulating hormone, estradiol and age is associated with the pregnancy outcome for women undergoing assisted reproduction: a retrospective cohort analysis. *Sci China Life Sci*. 2019;62(1):112–8.
- Zhu Q, Ma H, Wang J, Liang X. Understanding the mechanisms of diminished ovarian reserve: insights from genetic variants and regulatory factors. *Reprod Sci*. 2024;31(6):1521–32.
- Ata B, Seyhan A, Seli E. Diminished ovarian reserve versus ovarian aging: overlaps and differences. *Curr Opin Obstet Gynecol*. 2019;31(3):139–47.
- Ozcel MD. Dehydroepiandrosterone supplementation improves ovarian reserve and pregnancy rates in poor responders. *Eur Rev Med Pharmacol Sci*. 2020;24(17):9104–11.
- Cedars MI. Managing poor ovarian response in the patient with diminished ovarian reserve. *Fertil Steril*. 2022;117(4):655–6.
- Zhang QL, Lei YL, Deng Y, Ma RL, Ding XS, Xue W, et al. Treatment progress in diminished ovarian reserve: Western and Chinese Medicine. *Chin J Integr Med*. 2023;29(4):361–7.
- Li S, Hu L, Zhang C. Urinary vitamin D-binding protein as a marker of ovarian reserve. *Reprod Biol Endocrinol*. 2021;19(1):80.
- Wang H, Cao D, Wang M, Shi Y, Wei B, Jiang S, et al. Proteomic analysis of human follicular fluid reveals the pharmacological mechanisms of the Chinese patent drug Kunling pill for improving diminished ovarian reserve. *Evid Based Complement Alternat Med*. 2022;2022:5929694.
- Xu M, Li F, Xu X, Hu N, Miao J, Zhao Y, et al. Proteomic analysis reveals that cigarette smoke exposure diminishes ovarian reserve in mice by disrupting the CREB1-mediated ovarian granulosa cell proliferation-apoptosis balance. *Ecotoxicol Environ Saf*. 2024;271:115989.
- Humaidan P, La Marca A, Alviggi C, Esteves SC, Haahr T. Future perspectives of POSEIDON stratification for clinical practice and research. *Front Endocrinol (Lausanne)*. 2019;10:439.
- Shah IA, Memon M, Ansari S, Kumar R, Chandio SA, Mirani SH, et al. Role of coenzyme Q10 in prophylaxis of myocardial infarction. *Cureus*. 2021;13(2):e13137.
- Li HX, Xu XJ, Liu L. A new day 4 grading system to assess embryo quality in frozen embryo transfer cycles. *Reprod Sci*. 2021;28(5):1333–8.
- Dong L, Xin X, Chang HM, Leung PCK, Yu C, Lian F, et al. Expression of long noncoding RNAs in the ovarian granulosa cells of women with diminished ovarian reserve using high-throughput sequencing. *J Ovarian Res*. 2022;15(1):119.
- Li HX, Jing YX, Chai YH, Sun XH, He XX, Xue SL, et al. Mechanism of procyandin B2 in the treatment of Chronic Myeloid Leukemia based on integrating network pharmacology and molecular docking. *Anticancer Agents Med Chem*. 2023;23(16):1838–47.
- Lin G, Li X, Jin Yie SL, Xu L. Clinical evidence of coenzyme Q10 pretreatment for women with diminished ovarian reserve undergoing IVF/ICSI: a systematic review and meta-analysis. *Ann Med*. 2024;56(1):2389469.
- Jiang Z, Shen H. Mitochondria: emerging therapeutic strategies for oocyte rescue. *Reprod Sci*. 2022;29(3):711–22.
- Yang J, Liu Q, Yu B, Han B, Yang B. 4D-quantitative proteomics signature of asthenozoospermia and identification of extracellular matrix protein 1 as a novel biomarker for sperm motility. *Mol Omics*. 2022;18(1):83–91.
- Cozzolino M, Herraiz S, Titus S, Roberts L, Romeo M, Peinado I, et al. Transcriptomic landscape of granulosa cells and peripheral blood mononuclear cells in women with PCOS compared to young poor responders and women with normal response. *Hum Reprod*. 2022;37(6):1274–86.
- Cicchinelli M, Primiano G, Servidei S, Ardito M, Percio A, Urbani A, et al. Resolving phenotypic variability in mitochondrial diseases: preliminary findings of a proteomic approach. *Int J Mol Sci*. 2024;25(19):10731.
- Wang T, Xie X, Liu H, Chen F, Du J, Wang X, et al. Pyridine nucleotide-disulphide oxidoreductase domain 2 (PYROXD2): Role in mitochondrial function. *Mitochondrion*. 2019;47:114–24.
- Baradaran R, Berrisford JM, Minhas GS, Sazanov LA. Crystal structure of the entire respiratory complex I. *Nature*. 2013;494(7438):443–8.
- Stroud DA, Surgenor EE, Formosa LE, Reljic B, Frazier AE, Dibley MG, et al. Accessory subunits are integral for assembly and function of human mitochondrial complex I. *Nature*. 2016;538(7623):123–6.
- Ogilvie I, Kennaway NG, Shoubridge EA, et al. A molecular chaperone for mitochondrial complex I assembly is mutated in a progressive encephalopathy. *J Clin Invest*. 2005;115(10):2784–92.

29. Iwata S, Lee JW, Okada K, Lee JK, Iwata M, Rasmussen B, et al. Complete structure of the 11-subunit bovine mitochondrial cytochrome bc1 complex. *Science*. 1998;281(5373):64–71.
30. Hahn A, Parey K, Bublitz M, Mills DJ, Zickermann V, Vonck J, et al. Structure of a complete ATP synthase dimer reveals the molecular basis of inner mitochondrial membrane morphology. *Mol Cell*. 2016;63(3):445–56.
31. Ji Z, Liu GH, Qu J. Mitochondrial sirtuins, metabolism, and aging. *J Genet Genomics*. 2022;49(4):287–98.
32. Tasi YC, Chao HC, Chung CL, Liu XY, Lin YM, Liao PC, et al. Characterization of 3-hydroxyisobutyrate dehydrogenase, HIBADH, as a sperm-motility marker. *J Assist Reprod Genet*. 2013;30(4):505–12.
33. Fernandez-Vizarra E, Zeviani M. Mitochondrial disorders of the OXPHOS system. *FEBS Lett*. 2021;595(8):1062–106.
34. May-Panloup P, Boucret L, Chao de la Barca JM, Desquiret-Dumas V, Ferré-L'Hôtelier V, Morinière C, et al. Ovarian ageing: the role of mitochondria in oocytes and follicles. *Hum Reprod Update*. 2016;22(6):725–743.
35. Qin H, Qu Y, Li R, Qiao J. In vivo and In vitro matured oocytes from mice of advanced reproductive age exhibit alternative splicing processes for mitochondrial oxidative phosphorylation. *Front Endocrinol (Lausanne)*. 2022;26(13):816606.
36. Palmieri V, Bozzi M, Signorino G, Papi M, De Spirito M, Brancaccio A, et al. α -Dystroglycan hypoglycosylation affects cell migration by influencing β -dystroglycan membrane clustering and filopodia length: A multiscale confocal microscopy analysis. *Biochim Biophys Acta Mol Basis Dis*. 2017;1863(9):2182–91.
37. Bello V, Moreau N, Sirour C, Hidalgo M, Buisson N, Darribère T. The dystroglycan: nestled in an adhesome during embryonic development. *Dev Biol*. 2015;401(1):132–42.
38. Kakahara A, Maemura M, Hatano A, Matsumoto M, Tsukada YI. WDR74-mediated ribosome biogenesis and proteome dynamics during mouse preimplantation development. *Genes Cells*. 2025;30(1):e70001.
39. Boucret L, Chao de la Barca JM, Morinière C, Desquiret V, Ferré-L'Hôtelier V, Descamps P, et al. Relationship between diminished ovarian reserve and mitochondrial biogenesis in cumulus cells. *Hum Reprod*. 2015;30(7):1653–64.
40. Tal R, Seifer DB. Ovarian reserve testing: a user's guide. *Am J Obstet Gynecol*. 2017;217(2):129–40.
41. Wu H, Zhu R, Zheng B, Liao G, Wang F, Ding J, et al. Single-cell sequencing reveals an intrinsic heterogeneity of the preovulatory follicular microenvironment. *Biomolecules*. 2022;12(2):231.

Publisher's Note

Springer Nature remains neutral with regard to jurisdictional claims in published maps and institutional affiliations.